

# Water Resources Research®








## RESEARCH ARTICLE

10.1029/2023WR036698

## Zeta Potential of Supercritical CO<sub>2</sub>-Water-Sandstone Systems and Its Correlation With Wettability and Residual Subsurface Trapping of CO<sub>2</sub>

### Key Points:

- The first evaluated zeta potential at supercritical CO<sub>2</sub>-water interface is smaller than −14 mV
- The CO<sub>2</sub>-water zeta potential reflects the wetting state and is impacted by divalent cations
- Normalized zeta potential correlates with CO<sub>2</sub> saturation and is a powerful tool to evaluate residual CO<sub>2</sub> trapping in aquifers

Jan Vinogradov<sup>1,2</sup> , Miftah Hidayat<sup>2,3,4</sup> , Mohammad Sarmadivaleh<sup>3</sup> , David Vega-Maza<sup>2,5</sup> , Stefan Iglauer<sup>6</sup> , Lijuan Zhang<sup>7</sup>, Dajiang Mei<sup>7</sup>, and Jos Derksen<sup>2</sup>

<sup>1</sup>Department of Mechanical Engineering and Mechatronics, Ariel University, Ariel, Israel, <sup>2</sup>School of Engineering, University of Aberdeen, Aberdeen, UK, <sup>3</sup>Discipline of Petroleum Engineering, Curtin University, Kensington, WA, Australia, <sup>4</sup>Faculty of Mining and Petroleum Engineering, Institut Teknologi Bandung, Bandung, Indonesia, <sup>5</sup>School of Engineering, University of Valladolid, Valladolid, Spain, <sup>6</sup>School of Engineering, Edith Cowan University, Joondalup, WA, Australia, <sup>7</sup>School of Chemistry and Chemical Engineering, Shanghai University of Engineering Science, Shanghai, China

### Correspondence to:

J. Vinogradov,  
jan.vinogradov@abdn.ac.uk; janv@ariel.ac.il; janvin71@gmail.com

### Citation:

Vinogradov, J., Hidayat, M., Sarmadivaleh, M., Vega-Maza, D., Iglauer, S., Zhang, L., et al. (2024). Zeta potential of supercritical CO<sub>2</sub>-water-sandstone systems and its correlation with wettability and residual subsurface trapping of CO<sub>2</sub>. *Water Resources Research*, 60, e2023WR036698. <https://doi.org/10.1029/2023WR036698>

Received 11 NOV 2023  
Accepted 27 OCT 2024

### Author Contributions:

**Conceptualization:** Jan Vinogradov  
**Formal analysis:** Jan Vinogradov, Miftah Hidayat  
**Investigation:** Miftah Hidayat  
**Methodology:** Jan Vinogradov, Miftah Hidayat  
**Project administration:** Jan Vinogradov, Jos Derksen  
**Resources:** Jan Vinogradov, Mohammad Sarmadivaleh, Stefan Iglauer  
**Supervision:** Jan Vinogradov, Mohammad Sarmadivaleh, David Vega-Maza, Stefan Iglauer, Jos Derksen  
**Validation:** Jan Vinogradov, Miftah Hidayat, Mohammad Sarmadivaleh, Jos Derksen  
**Visualization:** Jan Vinogradov, Miftah Hidayat

**Abstract** Although CO<sub>2</sub> geological storage (CGS) is thought to be one of the most promising technologies to sequester the anthropogenic CO<sub>2</sub> to mitigate the climate change, implementation of the method is still challenging due to lack of fundamental understanding of controls of wettability, which is responsible for residual trapping of the gas and its flow dynamics. One of the key parameters that controls the wetting state is the zeta potential,  $\zeta$ , at rock-water and CO<sub>2</sub>-water interfaces.  $\zeta$  in systems comprising rocks, carbonated aqueous solutions and immiscible supercritical CO<sub>2</sub> have not been measured prior to this study, where we detail the experimental protocol that enables measuring  $\zeta$  in such systems, and report novel experimental data on the multi-phase  $\zeta$ . We also demonstrate for the first time that  $\zeta$  of supercritical CO<sub>2</sub>-water interface is negative with a magnitude greater than 14 mV. Moreover, our experimental results suggest that presence of multi-valent cations in tested solutions causes a shift of wettability toward intermediate-wet state. We introduce a new parameter that combines multi-phase  $\zeta$  and relative permeability endpoints to characterize the wetting state and residual supercritical CO<sub>2</sub> saturation. Based on these results, we demonstrate that  $\zeta$  measurements could serve as a powerful experimental method for predicting CGS efficiency and/or for designing injection of aqueous solutions with bespoke composition prior to implementing CGS to improve the residual CO<sub>2</sub> trapping in sandstone formations.

**Plain Language Summary** Extensive research has been conducted in the field of CO<sub>2</sub> geological storage (CGS). However, among a multitude of parameters that affect the efficiency of CGS, the system's wettability has been investigated empirically rather than from first principles. Fundamentally, wettability controls distribution of injected CO<sub>2</sub> and reservoir fluids in the pore space, as well as the flow dynamics of all fluids in target formations. One of the main forces controlling the wetting state is related to electrostatic interaction between rock-water and CO<sub>2</sub>-water interfaces, and the zeta potential is a property that describes these interactions. With the zeta potential dependence on the partial CO<sub>2</sub> pressure, water pH and chemical composition, and mineralogy, wettability can be characterized and/or modified prior to CO<sub>2</sub> injection using this interfacial property, thus enabling optimization of residual CO<sub>2</sub> trapping and significantly improving overall CGS efficiency. We have designed and for the first time carried out coreflooding experiments combined with single- and multi-phase zeta potential measurements at CGS conditions. We have introduced the normalized zeta potential which comprises two independent wettability indicators, and report a correlation between this property, the residual CO<sub>2</sub> saturation and wettability. Our results explain the underlying mechanisms of dependence of CO<sub>2</sub> saturation on experimental conditions.

© 2024. The Author(s).

This is an open access article under the terms of the [Creative Commons Attribution License](https://creativecommons.org/licenses/by/4.0/), which permits use, distribution and reproduction in any medium, provided the original work is properly cited.

## 1. Introduction

A major component in the transition toward net-zero energy involves the capture of CO<sub>2</sub> and its storage in geological formations termed CGS (Ali et al., 2022). To prevent CO<sub>2</sub> from leaking back to the surface, four

**Writing – original draft:** Jan Vinogradov  
**Writing – review & editing:**  
 Jan Vinogradov, Miftah Hidayat,  
 Mohammad Sarmadivaleh, Stefan Iglauer,  
 Lijuan Zhang, Dajiang Mei, Jos Derksen

trapping mechanisms are used: (a) structural trapping (a tight caprock acts as a barrier through which CO<sub>2</sub> cannot permeate), (b) residual trapping (CO<sub>2</sub> plume is split into many micrometer-sized bubbles which are immobilized by capillary forces in the pore network), (c) dissolution trapping (CO<sub>2</sub> dissolves in the formation brine), and (d) mineral trapping (CO<sub>2</sub> chemically reacts with the formation brine and/or reservoir rock to form solid precipitates). The two primary storage mechanisms during the first several hundreds of years are structural and residual trapping (Benson & Cole, 2008). The efficiency of these mechanisms is controlled by the CO<sub>2</sub>-Brine-Rock (CO<sub>2</sub>BR) wettability at equilibrium, which is established between the injected CO<sub>2</sub>, initially CO<sub>2</sub>-lean formation brines and minerals. Specifically, rock-wetting fluids tend to reside and flow in thin wetting layers along pore walls, which results in their lower residual saturation and lower relative permeability, thus affecting both, flow dynamics and trapped fluid volumes (Blunt et al., 2013; Collini & Jackson, 2022; Muggeridge et al., 2014). Thus, it is critically important to rigorously understand CO<sub>2</sub>-wettability, in order to optimize CGS for higher residual trapping of CO<sub>2</sub>. From a thermodynamics perspective, wettability is defined by stability of the wetting film at the solid surface, which is controlled by the total disjoining pressure, surface energy and capillary pressure. From first principles, the disjoining pressure comprises three main forces: structural (reflecting intermolecular structure of solvent), Van der Waals and electrostatic (Hirasaki, 1991). The former two are related to rock and fluid properties (topology of the pore space, refractive indices, permittivities, surface energy) as functions of reservoir conditions, have been routinely measured and, in general, are well known and characterized. The electrostatic force is also a function of reservoir conditions and rock mineralogy, but also depends on pH, composition and concentration of formation brines, all of which can theoretically be modified to yield optimal wettability (e.g., through injection of brines of specific chemical composition) thus enabling artificial control and/or improvement of CGS. The electrostatic force is characterized by a measurable interfacial quantity termed the zeta potential ( $\zeta$ ), the current knowledge of which in CO<sub>2</sub>BR systems is quite limited. Understanding  $\zeta$  in addition to other wettability controls (i.e., interfacial tension, refractive indices, permittivities, capillary pressure) will provide the necessary, as of now missing, link between experiments, theory and numerical simulations. Moreover, it has been demonstrated that  $\zeta$  measured in multi-phase experiments correlates with water saturation (Vinogradov & Jackson, 2011). Therefore,  $\zeta$  is useful for characterizing CO<sub>2</sub> saturation during the CGS, thus enabling process optimization.

On the fundamental level, when electrolytic solutions come in contact with solids or other fluids, the respective interfaces often develop a non-zero electric charge. To balance this surface charge, ions of the opposite polarity (counter-ions) are attracted from the bulk electrolyte toward the interface, thus forming an electrical double layer. Counter-ions that directly adsorb onto the mineral surface are immobile and form the so-called Stern layer, while those that are electrostatically attracted populate the diffuse part of the electrical double layer and can be mobilized by pressure, concentration or temperature gradients. Therefore, recognizing the importance of mobile counter-ions,  $\zeta$  is defined as the electric potential at the slip plane, which separates the immobile part of the electrical double layer from the mobile one. When excess counter-ions within the diffuse layer are mobilized by a flow, the so-called streaming current is established resulting in a separation of charge along the mineral surface. To maintain the overall electroneutrality, the corresponding and directly measurable streaming potential arises, from which  $\zeta$  can be interpreted and related to the wetting state.

An increasing number of studies have reported laboratory measurements of wettability characterized by directly measured contact angles (Iglauer et al., 2015), interpreted from volume-averaged rock properties (Krevor et al., 2012) or obtained from in situ X-ray micro-CT (Tudek et al., 2017). Other published studies have employed analytical methods (Tokunaga, 2012) or numerical models on multiple scales (Song et al., 2017; Yong et al., 2021) to evaluate the wetting state. However, many challenges still remain with respect to each method, reported data set or completeness of the investigated parameter space. At present, published laboratory experiments related to CGS cover a limited parameter space and do not look at cross-correlation of all fundamental parameters that define wettability. For instance, contact angle and interfacial tension measurements (Singh et al., 2016; Stevar et al., 2019) reported a limited number of values without providing fundamental explanation of observations, which would only be possible through inclusion of the critically important  $\zeta$  measured at the same experimental conditions.

More specifically, contact angles measured on quartz in contact with various aqueous solutions and supercritical CO<sub>2</sub> investigated effects of composition, concentration, pore pressure and temperature. However, the reported results are inconsistent with some studies reporting the contact angle to be independent of the pore pressure and temperature (Chen et al., 2015) while others reported increasing contact angles with pore pressure and temperature (Alnili et al., 2018). Several studies reported contact angles to be identical for solutions containing mono-

versus divalent cations (Chen et al., 2015), when other studies demonstrated increase in contact angles with  $\text{CaCl}_2$  and  $\text{MgCl}_2$  solutions relative to  $\text{NaCl}$  (Al-Yaseri et al., 2016). The concentration dependence of contact angles measured in such systems is also inconsistent with some papers reporting increasing contact angles with increasing concentration (Jung & Wan, 2012) and other studies reporting the opposite trend (e.g., Sarmadivaleh et al., 2015). Finally, many papers reported contact angles measured in quartz- $\text{CO}_2$ -water systems at CGS conditions to range between  $20^\circ$  and  $60^\circ$ , corresponding to water-wet conditions (e.g., Chen et al., 2015) while some other studies reported contact angles in seemingly identical systems to be in the range of  $75^\circ$  to  $95^\circ$ , thus corresponding to intermediate conditions (Bikkina, 2011; Sutjiadi-Sia et al., 2008).

Very few analytical studies relevant to CGS employed Derjaguin-Landau-Verwey-Overbeek (DLVO) theory to model wettability (Tokunaga, 2012). However, in the absence of established experimental data, these studies assumed the zeta potential at rock-water ( $\zeta_{r-w}$ ) and  $\text{CO}_2$ -water ( $\zeta_{c-w}$ ) interfaces, thus although being useful and insightful, their results were quite speculative.

Various micro-scale numerical modeling methods have been used to simulate  $\zeta$  and wettability of CGS systems, with two approaches considering the fundamental interfacial interactions: the molecular dynamics (MD) and surface complexation models (SCM). SCMs are effective in describing geochemical reactions and potentially are fully predictive (Vinogradov et al., 2022) for  $\zeta_{r-w}$ , but no such models have been tried for supercritical  $\text{CO}_2$ -water interface at CGS conditions. Classical MD models consider discrete molecules, ions and atoms, while explicitly simulating their interactions at supercritical  $\text{CO}_2$ -water interface on the atomic scale, which enables determination of contact angles, interfacial tension and/or other properties of interest (Silvestri et al., 2019). However, despite the merits of SCM and MD, both methods invoke multiple assumptions on still unavailable experimental values of  $\zeta_{c-w}$ , thus rendering these approaches speculative and uncertain. Moreover, these studies have not investigated the effect of flow dynamics or used their results to provide reliable and scalable input parameters for reservoir-scale simulations, which are used to assess the process efficiency.

Prior to implementing CGS, it is a common practice to use large-scale aquifer/reservoir simulation to assess the process efficiency. However, the available reservoir simulators compute  $\text{CO}_2$  saturation and flow dynamics using assumed sets of relative permeability functions, the shape of which strongly depends on the wetting state. At best, the relative permeability curves can be taken from a very limited set of laboratory experiments (Krevor et al., 2012), however the conditions of salinity, pore pressure, temperature, chemical composition, mineralogy and porous medium structure in the simulated formations are usually different from the respective laboratory studies and may be highly variable in space and time across the reservoir. Therefore, the physicochemical interactions at the  $\text{CO}_2$ -water and rock-water interfaces (which impact the wetting state through, in part, their effect on  $\zeta_{c-w}$ ,  $\zeta_{r-w}$ , and multi-phase  $\zeta_{m-p}$ ) are not fully captured in simulations, and relative permeability curves are not constantly updated, all of which results in highly uncertain predictions.  $\zeta_{m-p}$  obtained for rock samples saturated with both fluids is an effective property comprising contributions of individual water- $\text{CO}_2$  and rock-water interfaces with the corresponding  $\zeta_{c-w}$  and  $\zeta_{r-w}$ .

Several published studies investigated gas-water zeta potentials with air (Najafi et al., 2007) or  $\text{CO}_2$  (Kim & Kwak, 2017), but none of these studies managed to obtain reliable measurements at elevated temperature, high pressure or ionic strengths above  $10^{-2}$  M ( $\text{M} = \text{mol} \cdot \text{L}^{-1}$ ). Even at ambient conditions the reported zeta potentials of  $\text{CO}_2$ -water interfaces varied between nearly zero (Najafi et al., 2007), approximately  $-18$  mV (Kim & Kwak, 2017), and  $+10$  mV (Zhou et al., 2021) with  $10^{-3}$  M  $\text{NaCl}$  at the same pH value. One study (Moore et al., 2004) reported measurements of the zeta potential with intact rock samples saturated at high pressure with distilled water and liquid  $\text{CO}_2$  at irreducible water saturation. However, these results were obtained at  $20^\circ\text{C}$  and the reported zeta potentials were likely misinterpreted as discussed in by Vinogradov et al. (2021).

There have been only two studies that reported  $\zeta$  measurements at CGS conditions (Hidayat et al., 2022a, 2022b) but they were limited to a single-phase flow (rock saturated with fully carbonated solution at supercritical  $\text{CO}_2$  ( $\text{scCO}_2$ ) conditions, termed  $\text{C\_water}$ ), and none were complemented by relative permeability measurements, which relates to wettability,  $\text{scCO}_2$  saturation and determines  $\text{scCO}_2$  flow dynamics.

In summary, our predictive capabilities are currently limited: the experimental data are incomplete and cover a limited parameter space, the available data have not been interpreted in terms of the fundamental principles (i.e., various parameters were measured but not explained), the previously used analytical and numerical methods remain disconnected and are not based on verified evidence, and reservoir simulations are not coupled with

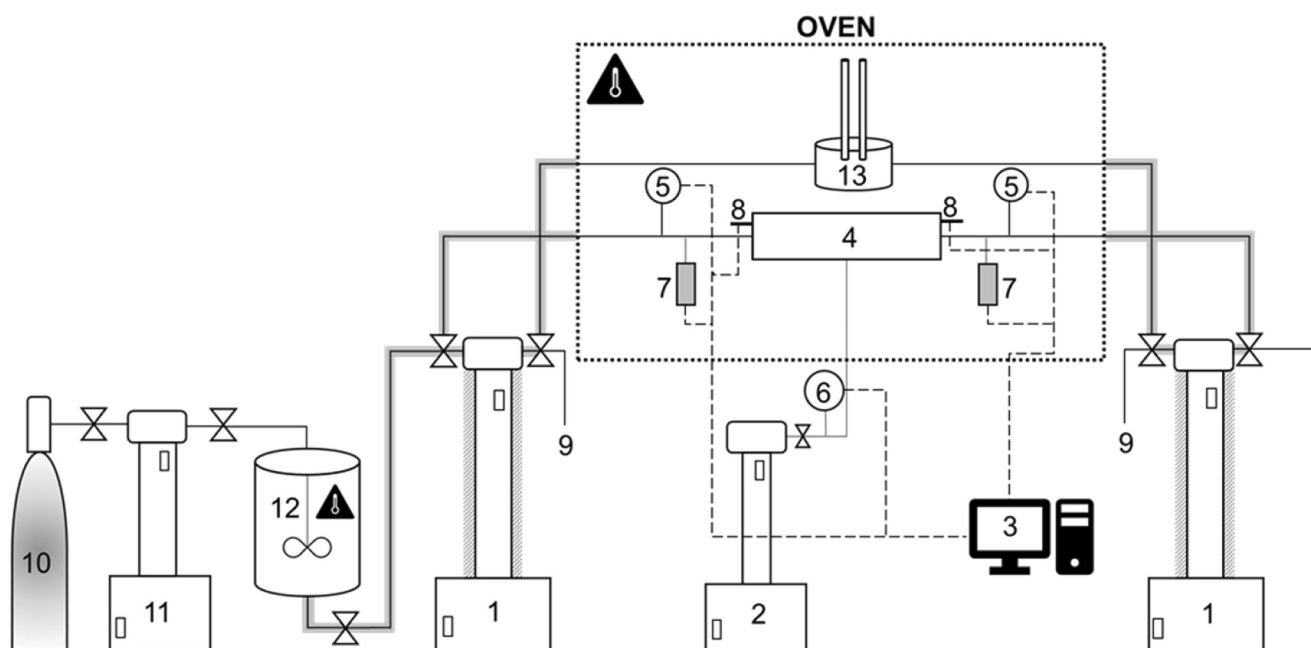


**Figure 1.** The experimental apparatus used in streaming potential measurements. The solid gray lines represent flowlines and the dashed gray lines represent electrical connections. (#1) heated 500D Hastelloy ISCO pumps to the left and to the right of the core holder; (#2) 500D is a stainless steel ISCO pump used to induce the confining pressure around the rock sample; (#3) data acquisition system; (#4) is the HPHT coreflooding cell (core holder); (#5) two high precision pressure transducers; (#6) high precision pressure transducer used to monitor the confining pressure; (#7) external electrodes to the left and to the right of the core holder; (#8) internal electrodes to the left and to the right of the core holder; (#9) are sampling tubes to the left and to the right of the core holder; (#10) CO<sub>2</sub> cylinder; (#11) 260D Stainless steel ISCO pump used for pumping CO<sub>2</sub> into the mixing reactor; (#12) heated Parr mixing reactor; (#13) high pressure in-line pH meter.

verified models or based on accurate experimental data and adequate assumptions. Therefore, although the subsurface formations suitable for implementation of CGS worldwide possess significant volumes to store large amounts of anthropogenic CO<sub>2</sub>, none of the current projects at their advanced development stages (apart from the Sleipner field in Norway, which is a depleted gas reservoir and outside of this study's scope) are operational. This is mainly due to poorly characterized dynamics of CO<sub>2</sub> saturation and flow, owing to inherently complex and heterogeneous geological constitution combined with a lack of understanding of highly complex physicochemical interactions between minerals and various fluids based on first principles.

In this study, we address the above shortcomings through pioneering targeted experiments that provide insights into controls of wettability and scCO<sub>2</sub> saturation. We report, for the first time,  $\zeta_{m-p}$  measured with various aqueous solutions at conditions corresponding to scCO<sub>2</sub>, and demonstrate the polarity and likely magnitude of  $\zeta_{c-w}$ . Furthermore, we report endpoints of relative permeability to water under these conditions and interpret the effective wetting state of a rock sample using two independent properties.

## 2. Materials and Methods

The experimental apparatus (Figure 1), the intact Fontainebleau sandstone sample (>99%wt quartz, liquid permeability of  $70 \pm 5$  mD, porosity of  $9 \pm 2\%$ , and intrinsic formation factor of  $58 \pm 2$ ) and C<sub>water</sub> solutions (all having the ionic strength of 0.05 M) used in this work (NaCl, NaC-10, CaCl<sub>2</sub>, MgCl<sub>2</sub>, Na<sub>2</sub>SO<sub>4</sub>) were identical to those reported in a previously published paper (Hidayat et al., 2022a; C<sub>water</sub> is termed live water in the study). The solutions' ionic strength was selected to be high enough to make the surface conductivity negligible (refer to Supplementary data in Hidayat et al., 2022a) and sufficiently low to keep the streaming potential measurable. Furthermore, in this initial study we conducted experiments with single salts containing mono- and di-valent anions and cations to investigate the effect of C<sub>water</sub> composition on  $\zeta$ . Future work is planned to expand the parameter space to include higher ionic strength and complex composition C<sub>water</sub> solutions.

The experimental protocol adopted in this study was modified from Hidayat et al. (2022a) to accommodate the multi-phase unsteady state displacement experiments, all of which were conducted at 40°C. Initial pressure

conditions for drainage (scCO<sub>2</sub> displaces C<sub>water</sub>) were identical to the corresponding preceding single-phase C<sub>water</sub> experiment (either 7.5 or 10 MPa). During the imbibition (C<sub>water</sub> solution displaces scCO<sub>2</sub>) stage, the same C<sub>water</sub> produced during drainage was reinjected into the core to minimize any disturbance to the established thermodynamic and chemical equilibrium between the rock and pore fluids. Our experiments replicate subsurface conditions that are established between minerals, the injected scCO<sub>2</sub> and formation brines, which become fully saturated with the gas during the equilibration.

We used a constant injection rate of 1 mL/min during unsteady state drainage and imbibition, so that the corresponding capillary number of  $Ca = 2.5 \times 10^{-8}$  was achieved at the end of drainage (when irreducible water saturation,  $S_{wirr}$ , was reached) and  $Ca = 3.2 \times 10^{-7}$ – $4.6 \times 10^{-7}$  was achieved at the end of imbibition (when residual gas saturation,  $S_{gr}$ , was reached). The capillary number, defined as  $Ca = \frac{u \times \mu}{\gamma}$  ( $u = \frac{Q}{A}$  is the Darcy velocity determined from the flow rate,  $Q$ , and cross-sectional area to the flow,  $A$ ;  $\mu$  is the dynamic viscosity of the flowing fluid;  $\gamma$  is the CO<sub>2</sub>-water interfacial tension) was evaluated at relevant experimental conditions to confirm the capillary dominated displacement.

The experimental protocol for measuring the streaming potential coupling coefficient as a function of C<sub>water</sub> saturation,  $C_{EK}(S_w)$ , consisted of the following steps:

1. During drainage 40 mL (approximately five pore volumes, PV) of pure scCO<sub>2</sub> were repeatedly injected into the rock sample initially fully saturated with C<sub>water</sub>. Between the injections the core holder (#4) was closed and disconnected from the rest of the setup to maintain the experimental temperature and pressure, the pumps (#1) were then used to flow C<sub>water</sub> through the in-line pH meter (#13) to measure pH of the effluent C<sub>water</sub>, the saturated rock conductivity ( $\sigma_{rw}$ ) was measured using the internal electrodes (#8), and volume of produced C<sub>water</sub> was measured in the depressurized receiving pump (assuming <1% change in density after reducing in-cylinder pressure to 100 kPa for the measurements (McBride-Wright et al., 2015)). The injections were repeated until no more C<sub>water</sub> was produced, hence  $S_{wirr}$  was reached.
2. After reaching the irreducible C<sub>water</sub> saturation,  $C_{EK}(S_{wirr})$  was obtained from measured stabilized pressure difference and voltage using the paired-stabilized method in one direction and the flow rate of 1 mL/min (Vinogradov & Jackson, 2011). In addition, one pressure-ramping experiment (Vinogradov & Jackson, 2011) with the maximum injection pressure of 20 kPa was conducted to confirm the value of  $C_{EK}(S_{wirr})$ . We limited the measurements to one flow rate and one pressure ramping test to maintain the water displacement in the capillary dominated regime.
3. Upon completion of  $C_{EK}(S_{wirr})$  evaluation, the rock sample was allowed to age with scCO<sub>2</sub> for 7 days to allow wettability alteration to take place (with longer aging period the measuring electrodes (#8) were observed to become unstable, likely due to an impact of low pH on the electrode surface reactions, hence we limited the aging to 7 days for all experiments).
4. During subsequent imbibition 2.5 PV of C<sub>water</sub> were injected into the sample saturated with C<sub>water</sub> and immiscible scCO<sub>2</sub>. The core holder was then closed, pH of the effluent C<sub>water</sub> and saturated rock conductivity ( $\sigma_{rw}$ ) were measured, the receiving pump was depressurized and volume of produced C<sub>water</sub> was measured. The above injection steps were repeated until volume of produced C<sub>water</sub> became equal to the volume of the injected C<sub>water</sub> (volume of produced scCO<sub>2</sub> was calculated as a difference between the injected and produced C<sub>water</sub> volumes), hence residual gas saturation,  $S_{gr}$  ( $S_w = 1 - S_{gr}$ ), was reached.
5. At this stage,  $C_{EK}(1 - S_{gr})$  for all tested solutions was obtained using the paired-stabilized method with the flow rate of 1 mL/min both directions to allow continuous monitoring of produced volumes of C<sub>water</sub> and pH and to maintain the displacement within the capillary dominated regime. Furthermore, at least three pressure-ramping experiments with the maximum injection pressure of up to 20 kPa were also conducted at this stage to acquire independent evaluation of  $C_{EK}(1 - S_{gr})$ . Note that there was no additional CO<sub>2</sub> production in the receiving pump at any point. Constant  $S_w = 1 - S_{gr}$  during the last step was also independently confirmed via regular measurements of relative permeability to C<sub>water</sub>,  $\sigma_{rw}$  and  $C_{EK}$ , all of which remained constant.
6. Finally, we conducted additional paired-stabilized experiments using at least four different flow rates between 4 mL/min and 12 mL/min with an increment of 2 mL/min. The first of these multi-rate experiments was conducted at the highest rate of 12 mL/min (the so-called “high-rate bump”) in the same flow direction as during step 4. This first high-rate bump was carried out to eliminate or reduce the capillary end effects (if there were any) while still enabling measuring volumes of produced C<sub>water</sub>. Upon completion of the first high-rate bump, additional multi-rate paired-stabilized experiments were carried out in both directions to allow a more

accurate interpretation of  $C_{EK}(1 - S_{gr})$  (Vinogradov et al., 2010). Due to technical restrictions of the experimental setup (e.g., requirement to disconnect the core holder from the rest of the setup after each pumping; necessity to depressurize the receiving pump to measure volumes of produced C<sub>water</sub> with subsequent refilling of the pump with fresh C<sub>water</sub> for the next experiment; extremely time consuming nature of each test resulting in a loss of the electrode stability) the final C<sub>water</sub> saturations ( $S_w = 1 - S_{gr}$ ) in multi-rate tests were updated from the values obtained during step 5 only once at the end the first paired-stabilized experiment conducted at the highest flow rate of 12 mL/min.

All experiments were carried out at chemical and thermal equilibrium between rock, C<sub>water</sub> and scCO<sub>2</sub> to replicate reservoir conditions post CO<sub>2</sub> injection when the fluids and minerals are already at equilibrium. During the entire experiment the chemical equilibrium of the system was monitored by continuous measurements of pH, which remained constant and stable (2% tolerance) for the entire duration of drainage and/or imbibition (i.e., at least for 7–10 days). In addition, the equilibrium was also confirmed at  $S_{wirr}$  and  $S_w = 1 - S_{gr}$  by measurements of  $C_{EK}$  and  $\sigma_{rw}$  as described above, both of which remained constant and stable (2% tolerance) over a period of at least 2 days.

All dead volumes (flowlines connecting pumps to the core holder, valves, etc.) were accurately measured prior to conducting the multi-phase experiments. Precisely measured volumes of injected and produced fluids combined with the measured dead volumes and sample porosity were used to compute the average water saturation at the end of each scCO<sub>2</sub> or C<sub>water</sub> injection.

To calculate the zeta potential at  $S_w = 1$  and residual gas saturation ( $S_w = 1 - S_{gr}$ ) we used the classical Helmholtz-Smoluchowski (HS) equation

$$C_{EK} = \frac{\Delta V}{\Delta P} = \frac{\epsilon \zeta}{\mu \sigma_w} \quad (1)$$

where  $\Delta V$  is the measured voltage (i.e., the streaming potential) across the rock sample,  $\Delta P$  is the pressure difference,  $\epsilon$  is the dielectric constant of the C<sub>water</sub>,  $\mu$  is C<sub>water</sub> dynamic viscosity,  $\sigma_w$  is the effective electrical conductivity of C<sub>water</sub>, and  $\zeta$  is the zeta potential.

In this study,  $\zeta_{r-w}$  and  $\zeta_{m-p}$  were interpreted from direct  $C_{EK}$  measurements (voltage and pressure difference) carried out on samples saturated with C<sub>water</sub>, and C<sub>water</sub> with residual scCO<sub>2</sub>, respectively. Polarity and the likely magnitude of  $\zeta_{c-w}$  were interpreted from the difference between  $\zeta_{r-w}$  and  $\zeta_{m-p}$ , as detailed in Sections 4.1 and 4.2.

### 3. Results

#### 3.1. Multi-Phase Streaming Potential Coupling Coefficient, $C_{EK}$ , at $S_{wirr}$ and $S_w = 1 - S_{gr}$

We begin from reporting  $C_{EK}$  (Figure 2) interpreted from pressure difference and voltage measurements for single- (both, dead, i.e. saturated with CO<sub>2</sub> at atmospheric pressure and temperature in Figure 2a and C<sub>water</sub> in Figure 2b solutions) and multi-phase (C<sub>water</sub> in contact with rock and scCO<sub>2</sub>) systems. Specifically, values of the stabilized voltage (e.g., voltage averaged between 1,500 and 2,100 s in Figure 2a) were plotted against the corresponding values of the stabilized pressure for all tested flow rates, so that the slope of a linear regression yielded  $C_{EK}$ . Note that single-phase experiments correspond to water saturation  $S_w = 1$ . The stability of the internal electrodes used in our multi-phase experiments was considerably poorer compared with the single-phase dead or live solution experiments. The poorer electrode stability, therefore, resulted in increased noise level relative to the measured signal and hence, increased experimental errors as demonstrated in Figure 2. The experimental uncertainties associated with a higher noise level and poorer stability of measured voltage are reflected in the cumulative errors in the streaming potential coupling coefficient,  $C_{EK}$  (and consequently  $\zeta$ ), which followed the high-to-low order: Na<sub>2</sub>SO<sub>4</sub> → NaCl-10 → MgCl<sub>2</sub> → CaCl<sub>2</sub> → NaCl (NaCl-10 corresponds to the experiments carried out with live NaCl solution at the average pore pressure of 10 MPa, while the rest of the experiments were conducted at 7.5 MPa).

In multi-phase experiments a non-zero  $C_{EK}$  was recorded at residual gas saturation ( $S_w = 1 - S_{gr}$ ) while zero  $C_{EK}$  was observed in all experiments at irreducible C<sub>water</sub> or dead solution saturation ( $C_{EK}(S_{wirr}) = 0$  mV/MPa), Figures 2c and 2e. The zero  $C_{EK}(S_{wirr})$  reported here is consistent with the hypothesis that the streaming current

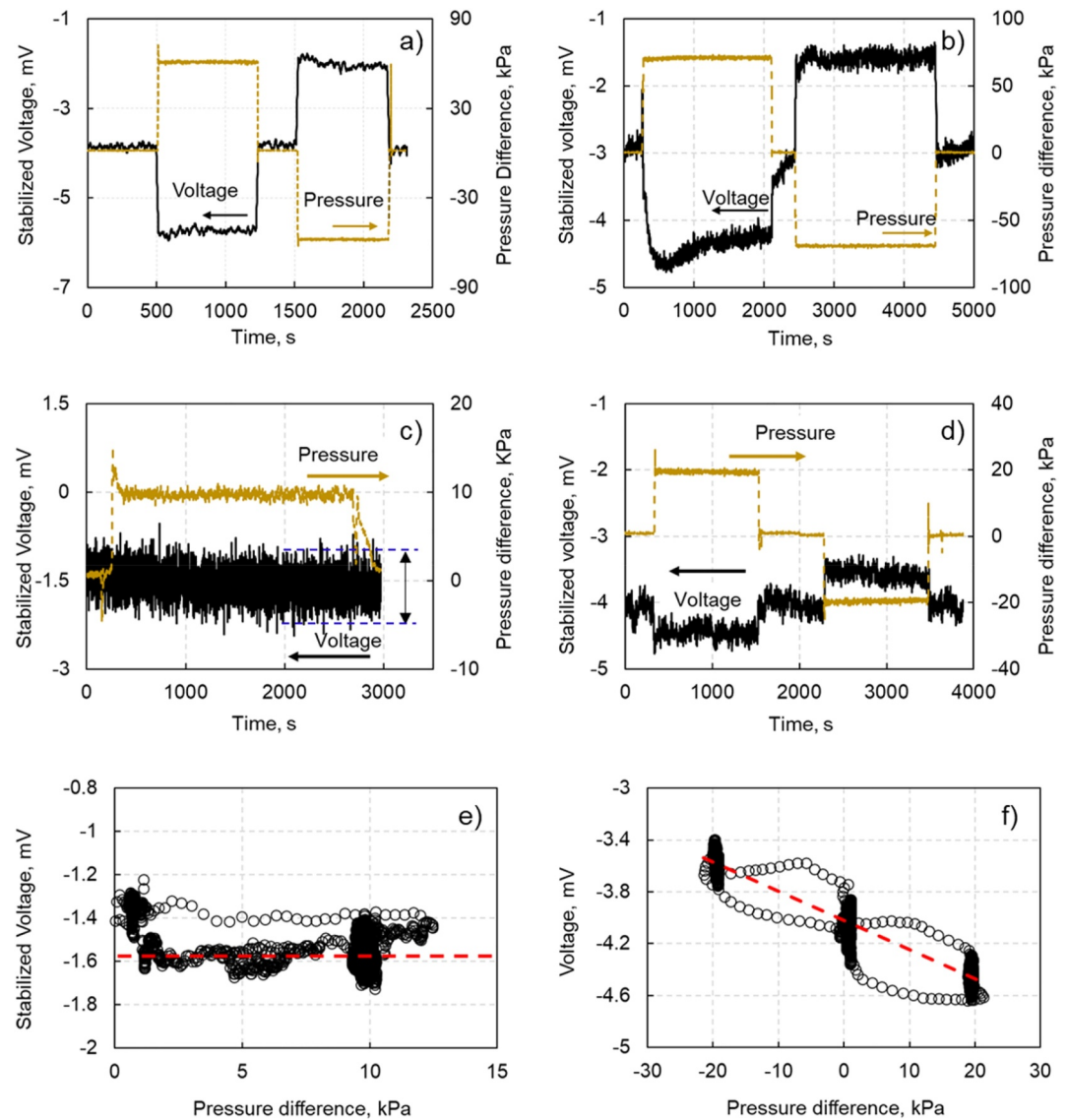


**Figure 2.** Typical results of the paired-stabilized experiments carried out with: (a) single-phase experiment with dead NaCl solution pumped at 4 mL/min, pore pressure of 7.5 MPa and temperature of 23°C (all data for dead solutions is available in Hidayat et al. (2022a) and presented here only for comparison in the voltage noise level); (b) single-phase experiment with NaCl C<sub>water</sub> solution pumped at 6 mL/min, pore pressure of 7.5 MPa and temperature of 40°C; (c) multi-phase paired-stabilized experiment with scCO<sub>2</sub> pumped at 1 mL/min in presence of NaCl C<sub>water</sub> solution at irreducible  $S_{wirr}$ , pore pressure of 7.5 MPa and temperature of 40°C; (d) multi-phase paired-stabilized experiment with NaCl C<sub>water</sub> solution pumped at 1 mL/min in presence of scCO<sub>2</sub> at  $S_w = 1 - S_{gr}$ , pore pressure of 7.5 MPa and temperature of 40°C; (e) multi-phase pressure-ramping experiment with scCO<sub>2</sub> pumped in presence of NaCl C<sub>water</sub> solution at irreducible saturation ( $S_{wirr}$ ), pore pressure of 7.5 MPa and temperature of 40°C; (f) multi-phase pressure-ramping experiment with NaCl C<sub>water</sub> solution pumped with maximum pressure of 20 kPa in presence of scCO<sub>2</sub> at  $S_w = 1 - S_{gr}$ , pore pressure of 7.5 MPa and temperature of 40°C. Slopes of the linear regressions, represented by the red dashed lines in panels (e) and (f) correspond to the respective values of  $C_{EK}$ .

should always be zero when C<sub>water</sub> or dead solution is at irreducible saturation and therefore immobile, the hypothesis that was confirmed by an analytical model (Vinogradov et al., 2021). Moreover, another experimental study (Vinogradov & Jackson, 2011) came to the same conclusion and attributed their non-zero  $C_{EK}(S_{wirr})$ , measured in sandstone samples saturated with water and undecane, to the experimental artifact, when very small (hence, unmeasurable) volumes of water were still produced at the end of drainage, thus contributing to the non-

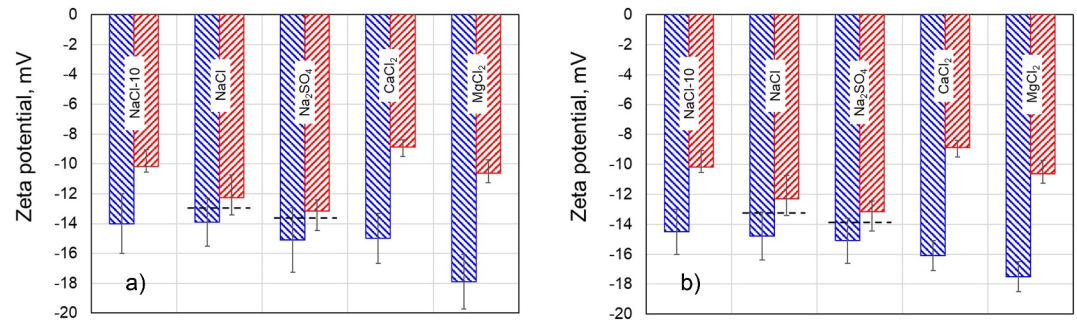


**Figure 3.**  $\zeta_{r-w}$  (red) and  $\zeta_{m-p}$  (blue) zeta potentials measured for CO<sub>2</sub>BR systems. NaCl-10 corresponds to the experiments conducted at 10 MPa, while the rest of the data were obtained at 7.5 MPa of the pore pressure. Panel (a) shows results obtained at the end of the imbibition stage and prior to carrying out multi-rate paired-stabilized experiments; Panel (b) shows the results obtained at the end of multi-rate tests. The dashed lines for some experiments demonstrate how  $\zeta_{m-p}$  and  $\zeta_{r-w}$  are seen as equal within the experimental errors.

zero flow of water and streaming current. For more detailed information on the interpretation of  $C_{EK}$  from measured pressure difference and voltage, please refer to Vinogradov et al. (2010) and Vinogradov and Jackson (2011).

### 3.2. Multi-phase Zeta Potential, $\zeta_{m-p}$ , at $S_w = 1 - S_{gr}$

In Equation 1 used to calculate  $\zeta_{m-p}$ ,  $C_{EK}$  was interpreted from directly measured response of voltage to applied pressure difference at the end of imbibition (Figures 2d and 2f), while viscosity, dielectric constant and  $C_{water}$  electrical conductivity ( $\mu$ ,  $\epsilon$  and  $\sigma_w$ ) were taken from the respective single-phase  $C_{water}$  experiments (Hidayat et al., 2022a). Note, that it was experimentally confirmed that surface electrical conductivity of all solutions was negligible at ionic strength of 0.05 M, thus allowing us to use  $\sigma_w$  as the effective water conductivity (refer to Supplementary data in Hidayat et al., 2022a).

All properties measured in the experiments along with cumulative experimental uncertainties for each property, both at the end of a single-rate imbibition experiment (step 5) and at the end of multi-rate tests (step 6), are reported in subsequent sections while Figure 3 shows  $\zeta_{m-p}$  (at  $S_w = 1 - S_{gr}$ ) of all tested systems along with their respective  $\zeta_{r-w}$  (at  $S_w = 1$ ) values.

The effective  $\zeta_{m-p}$  (with both scCO<sub>2</sub> and  $C_{water}$  present in the pore space) of systems containing  $C_{water}$  solutions of NaCl and Na<sub>2</sub>SO<sub>4</sub> at residual scCO<sub>2</sub> saturation ( $S_{gr}$ ) were found to be identical to their respective  $\zeta_{r-w}$  (only  $C_{water}$  occupies the pore space) values within the experimental uncertainty (Figure 3). However,  $\zeta_{m-p}$  for NaCl-10, CaCl<sub>2</sub> and MgCl<sub>2</sub> solutions were significantly different from  $\zeta_{r-w}$ , hence clearly indicating that  $\zeta_{m-p}$  in these experiments were influenced by the scCO<sub>2</sub>- $C_{water}$  interfaces and the corresponding  $\zeta_{c-w}$ . A more detailed analysis and interpretation of these results is provided in Sections 4.1 and 4.2.

Furthermore, the total change in  $S_w$  during the single-rate imbibition (step 5) ( $\Delta S_w = 1 - S_{gr} - S_{wirr}$ ) was found to be different across tested salts and pore pressure values so that:  $\Delta S_w(\text{NaCl} - 10) > \Delta S_w(\text{NaCl}) > \Delta S_w(\text{Na}_2\text{SO}_4) > \Delta S_w(\text{MgCl}_2) > \Delta S_w(\text{CaCl}_2)$ . As described in step 6 of the experimental protocol, at the end the first paired-stabilized experiment conducted at the highest flow rate of 12 mL/min  $S_{gr}$  was measured and did decrease compared to the values obtained from step 5 only for CaCl<sub>2</sub> and MgCl<sub>2</sub>. The corresponding  $\zeta_{m-p}$  obtained at the end of multi-rate tests however, remained equal to those from the single rate imbibition as shown in Figure 4a. The dashed lines in Figure 4a represent the variation of  $\zeta_{m-p}$  that corresponds to the experimental sequence: (a)  $\zeta_{r-w}$  was obtained for all systems when rock samples were fully saturated with  $C_{water}$  ( $S_w = 1$ ); (b)  $\zeta_{m-p} = 0$  was recorded at the end of drainage ( $S_w = S_{wirr}$ ); (c)  $\zeta_{m-p}$  values at the end of single- (step 5) and multi-rate (step 6) imbibition experiments and equal to those shown in Figures 3a and 3b, respectively. Note, that a change in  $S_w$  after the high-rate bump (measured once, after completion of the first injection of  $C_{water}$  at the highest rate of 12 mL/min) was recorded to be outside of the experimental error only for



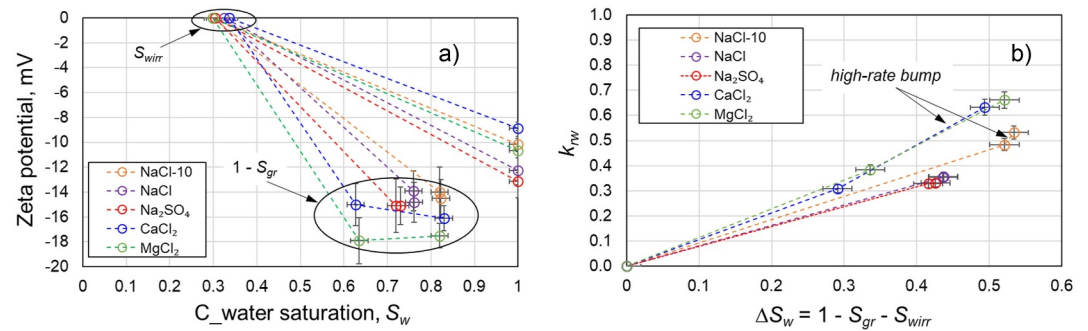


**Figure 4.**  $C_{\text{water}}$  saturation dependence of (a)  $\zeta_{m-p}$  and (b) relative permeability to  $C_{\text{water}}$  for all  $\text{CO}_2\text{-BR}$  systems. NaCl-10 corresponds to the experiments conducted at 10 MPa, while the rest of the data were obtained at 7.5 MPa of the pore pressure. The error bars for  $\zeta_{m-p}$  are identical to those shown in Figure 3 while the error bars for  $S_w$  and  $k_{rw}$  represent the accuracy of respective measurements.

$\text{CaCl}_2$  and  $\text{MgCl}_2$  solutions, while all values of  $\zeta_{m-p}$  at  $S_w = 1 - S_{gr}$  (measured at the end of paired-stabilized experiments) were found to be identical to the values recorded at the end of step 5.

Since  $S_{wirr}$  was slightly different in different tested systems, Figure 4b shows relative permeability to  $C_{\text{water}}$  as a function of  $S_w$  change ( $\Delta S_w$ ) from  $S_{wirr}$  to  $1 - S_{gr}$  in all systems. It should be noted that the lower values of  $\Delta S_w$  correspond to the single-rate imbibition (step 5), while the high-rate pumping induced changes in  $k_{rw}$  and  $1 - S_{gr}$  beyond the experimental uncertainty were only observed with  $\text{CaCl}_2$  and  $\text{MgCl}_2$ . These changes were also observed to a much lesser extent with NaCl-10, for which the change in  $k_{rw}$  was greater than the experimental error while the change in  $1 - S_{gr}$  was within the experimental uncertainty.

We attribute the above observations to different wetting states and different  $S_w$  of the systems affected by salt type and experimental pressure, all of which will be discussed in more detail in the following sections.

### 3.3. Role of pH in Controlling $\zeta_{c-w}$ and $\zeta_{m-p}$

To investigate the impact of pH on  $\zeta_{m-p}$  all measured values were plotted against the corresponding pH of  $C_{\text{water}}$  solutions and compared with  $\zeta_{r-w}$  values obtained under identical conditions in Figure 5.

It can be seen, that unlike the single-phase  $\zeta_{r-w}$ , the respective  $\zeta_{m-p}$  did not have any apparent dependence on pH. Specifically,  $\zeta_{m-p}$  for  $\text{CaCl}_2$ , NaCl-10, NaCl and  $\text{Na}_2\text{SO}_4$  were independent of pH, while the value for  $\text{MgCl}_2$  was the only outlier with a more negative  $\zeta_{m-p}$  compared with all other multi-phase values.

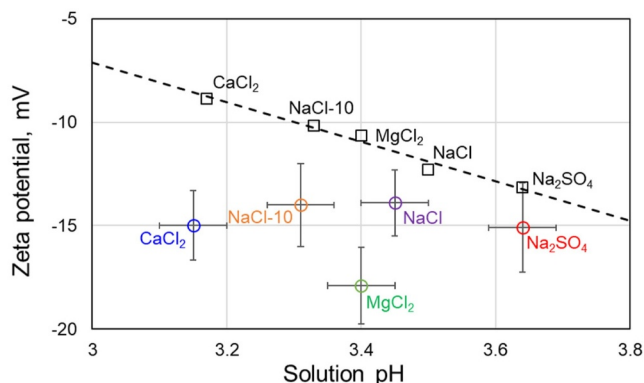


**Figure 5.** Multi- (colored symbols) and single-phase (black symbols) zeta potentials measured for  $C_{\text{water}}\text{-CO}_2\text{-sandstone}$  systems. The dashed line represents the pH dependence of single-phase  $C_{\text{water}}$  zeta potentials, which is identical to the one reported by Hidayat et al. (2022a).

The measured  $\zeta_{m-p}$  reflects combined individual contributions of  $\zeta_{r-w}$  and  $\zeta_{c-w}$ , thus being dependent on the system's wetting state. At the same time, there have been no studies that reported directly measured  $\zeta_{c-w}$  under CGS conditions, thus the effect of salt type and pore pressure on  $\zeta_{c-w}$  is unknown. Hence, the pH dependence of  $\zeta_{c-w}$  and/or  $\zeta_{m-p}$  could not be assumed similar to that of  $\zeta_{r-w}$  (given by Equation 5 in Hidayat et al., 2022a) or to align with the empirical trend reported for  $\text{CO}_2$  nanobubbles in water solutions at ambient conditions (Zhou et al., 2021).

Ultimately,  $\zeta_{m-p}$  reflects which fluid ( $C_{\text{water}}$  or  $\text{scCO}_2$ ) wets the pore wall thus determining with interfacial zeta potential ( $\zeta_{c-w}$  or  $\zeta_{r-w}$ ) will have more significant contribution to the effective multi-phase  $\zeta_{m-p}$ . On the other hand,  $\zeta_{m-p}$ , as well as  $\zeta_{c-w}$  or  $\zeta_{r-w}$ , depend on the system's pH. While the pH dependence of  $\zeta_{r-w}$  for  $\text{CO}_2\text{-BR}$  systems has been investigated (Hidayat et al., 2022a), the dependence of  $\zeta_{c-w}$  on pH at CGS conditions has not been reported. If the dependence of  $\zeta_{c-w}$  on pH and salt type at  $\text{scCO}_2$  conditions was similar to that at ambient pressure and temperature (Zhou et al., 2021), and of the same order as  $\zeta_{r-w}$  (Hidayat et al., 2022a) (both studies suggest that zeta

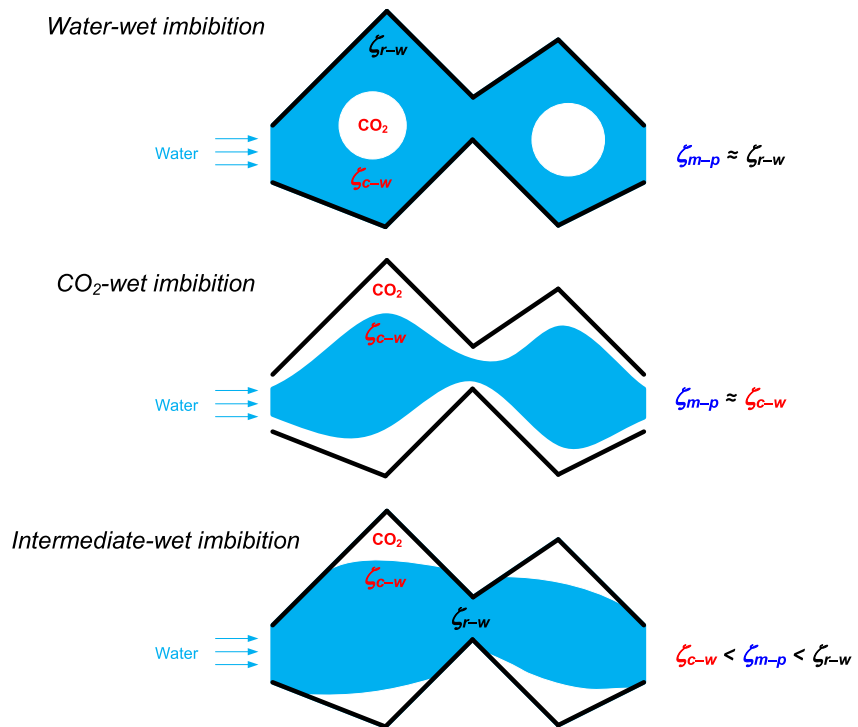


**Figure 6.** Qualitative description of fluids distribution in the pore space by the end of the imbibition displacement for three distinct wetting states. The individual zeta potentials at C<sub>2</sub>-water-rock ( $\zeta_{r-w}$ ) and scCO<sub>2</sub>-C<sub>2</sub>-water ( $\zeta_{c-w}$ ) interfaces are shown in black and red colors, respectively. The resulting multi-phase zeta potential ( $\zeta_{m-p}$ ) estimates are shown to the right, based on the experimentally confirmed conclusion that  $\zeta_{c-w}$  is negative and larger in magnitude than  $\zeta_{r-w}$ .

potentials become more positive with decreasing pH and with presence of divalent cations), the resulting dependence of  $\zeta_{m-p}$  on pH would be comparable to respective pH dependence of  $\zeta_{r-w}$  represented by the dashed line in Figure 5. That was not the case and therefore, we conclude that the measured  $\zeta_{m-p}$  were more strongly impacted by the pore space occupancy by scCO<sub>2</sub> rather than the pH.

## 4. Discussion

### 4.1. Polarity and Magnitude of scCO<sub>2</sub>-C<sub>2</sub>-water Zeta Potential, $\zeta_{c-w}$

The  $\zeta_{m-p}$  at  $S_w = 1 - S_{gr}$  results from the streaming current induced by a flow of C<sub>2</sub>-water along surfaces with a non-zero electrical charge, which in the pore space can develop at either the C<sub>2</sub>-water-rock or scCO<sub>2</sub>-C<sub>2</sub>-water interface. Therefore,  $\zeta_{m-p}$  depends on: (a) polarity and magnitude of  $\zeta_{r-w}$  (previously measured and reported for identical systems and conditions in Hidayat et al., 2022a) and  $\zeta_{c-w}$  (unknown); (b) distribution of scCO<sub>2</sub> in the pore space as depicted in Figure 6.

Specifically,  $\zeta_{c-w}$  is expected to have a stronger impact on  $\zeta_{m-p}$  at  $S_w = 1 - S_{gr}$  when C<sub>2</sub>-water is flowing only along continuous scCO<sub>2</sub> wetting films, thus corresponding to CO<sub>2</sub>-wet conditions. In this case, the only contribution to the measured multi-phase streaming potential, from which  $\zeta_{m-p}$  is interpreted, should come exclusively from the excess counter-ions moving along the scCO<sub>2</sub>-C<sub>2</sub>-water interface. And therefore,  $\zeta_{m-p}$  should be of the same polarity and magnitude as  $\zeta_{c-w}$ . Conversely, when immobile scCO<sub>2</sub> is trapped in the middle of the pores (water-wet conditions), the resulting multi-phase streaming potential should not be significantly affected by the discontinuous scCO<sub>2</sub>-C<sub>2</sub>-water interfaces and the resulting  $\zeta_{m-p}$  should be of order of  $\zeta_{r-w}$ . Finally, for intermediate-wet systems,  $\zeta_{m-p}$  should attain a value between  $\zeta_{r-w}$  and  $\zeta_{c-w}$ . These arguments were experimentally confirmed for crude oil-rock-brine systems (Collini & Jackson, 2022), so that a similar relationship between  $\zeta_{m-p}$ , taken relative to the corresponding  $\zeta_{r-w}$ , and the wetting state of CO<sub>2</sub>BR systems could be identified.

Many studies have measured contact angles in quartz-C<sub>water</sub>-scCO<sub>2</sub> systems. However, there is no clear consistency between the reported results. Some papers reported contact angles below 60° regardless of pore pressure, C<sub>water</sub> concentration or salt type (e.g., Sarmadivaleh et al., 2015). At the same time other papers showed that contact angles with scCO<sub>2</sub> and de-ionized water on quartz substrates varied between 45° and 95° corresponding to water-wet and intermediate-wet conditions, respectively (Bikkina, 2011). Chen et al. (2015) reported measurements with NaCl and CaCl<sub>2</sub> solutions and demonstrated that the contact angles remained below 30° and independent of salt type and pore pressure. In contrast, Al-Yaseri et al. (2016) reported larger contact angles for CaCl<sub>2</sub> and MgCl<sub>2</sub> relative to NaCl with all contact angles increasing with the pore pressure. Finally, Chiquet et al. (2007) reported a transition from water-wet to intermediate-wet conditions with NaCl solutions.

Considering the anticipated relationship between  $\zeta_{m-p}$  and wettability, along with the results presented in Figure 3 and three distinct wetting states described in Figure 6, we could conclude that presence of scCO<sub>2</sub> in NaCl-10, CaCl<sub>2</sub> and MgCl<sub>2</sub> systems led to some wettability alteration, evidenced by a significant difference between  $\zeta_{r-w}$  and  $\zeta_{m-p}$  caused by a substantial contribution of  $\zeta_{c-w}$ . Keeping in mind that  $\zeta_{c-w}$  could not be directly inferred from our experiments and the complete wetting of rock by scCO<sub>2</sub> was unlikely (the maximum contact angles found in the literature are in the range 82°–95°; Bikkina, 2011), only the case where  $\zeta_{r-w}$  and  $\zeta_{c-w}$  had the same polarity and significantly different magnitudes allowed us to unambiguously interpret  $\zeta_{c-w}$  from the difference between  $\zeta_{m-p}$  and  $\zeta_{r-w}$ . That is, if  $\zeta_{m-p}$  was found to be of the same polarity and *larger* in magnitude compared with  $\zeta_{r-w}$  (as was the case in our experiments), it would imply that  $\zeta_{c-w}$  also possessed the same polarity and was larger in magnitude than  $\zeta_{r-w}$ . In all other cases the interpretation of  $\zeta_{c-w}$  polarity and magnitude would be ambiguous if not impossible. For instance, if  $\zeta_{m-p}$  was of the same polarity but smaller in magnitude compared with  $\zeta_{r-w}$ , it could be equally possible for  $\zeta_{c-w}$  to be zero, negative and small, or positive.

Given that  $\zeta_{r-w}$  for all tested solutions and conditions were negative, we assumed a decreasing water wetness with increased pore pressure (NaCl to NaCl-10) and with the presence of divalent cations (CaCl<sub>2</sub> and MgCl<sub>2</sub>). Thus, following the above arguments, the effective  $\zeta_{m-p}$  would be of the same magnitude and polarity as  $\zeta_{c-w}$  in more scCO<sub>2</sub>-wet systems, while in intermediate-wet systems  $\zeta_{m-p}$  would gain the magnitude between  $\zeta_{c-w}$  and  $\zeta_{r-w}$ . Based on the results presented in Figure 3, both wetting states could correspond to NaCl-10, CaCl<sub>2</sub> and MgCl<sub>2</sub> experiments. In water-wet systems  $\zeta_{m-p}$  would have the same polarity and magnitude as  $\zeta_{r-w}$ , as was observed in our NaCl and Na<sub>2</sub>SO<sub>4</sub> experiments. However, the polarity and magnitude of  $\zeta_{c-w}$  could not be unambiguously inferred from these two experiments.

It is generally accepted that  $\zeta_{c-w}$  is primarily controlled by pH (Kim & Kwak, 2017), and since acidity of all tested multi-phase systems remained nearly identical, it was concluded that  $\zeta_{c-w}$  in NaCl and Na<sub>2</sub>SO<sub>4</sub> were also negative. Combining the results presented in Figure 3, the interpretation of impact of the wetting state on  $\zeta_{m-p}$  and reported measured contact angles, we concluded that the likely wetting state of NaCl-10, CaCl<sub>2</sub> and MgCl<sub>2</sub> systems corresponded to the weakly water-wet or intermediate-wet conditions. The wetting state of NaCl and Na<sub>2</sub>SO<sub>4</sub> systems corresponded to either strongly water-wet or weakly water-wet conditions with negative  $\zeta_{c-w}$  in all systems.

Considering the magnitude of  $\zeta_{m-p}$  relative to  $\zeta_{r-w}$  (Figure 3), showing that contribution of  $\zeta_{c-w}$  resulted in a more negative value of  $\zeta_{m-p}$ , we conclude that  $\zeta_{c-w} \leq -14$  mV in our experiments. However, since  $\zeta_{m-p}$  alone was insufficient to distinguish between the wetting states of different systems, further analysis was conducted to evaluate the wettability and other factors that affected  $\zeta_{m-p}$ .

#### 4.2. Normalized Zeta Potential, Wettability and Residual CO<sub>2</sub> Saturation

Due to high pressure and elevated temperature conditions of the experiments, it was impossible to directly measure the system's wettability using conventional methods that rely on spontaneous and forced imbibition cycles (Amott Wettability Index, or USBM). Therefore, to quantify the wettability we considered two independent parameters: the reciprocal scaled zeta potential,  $\zeta_{RS}$ ; and the reciprocal relative permeability gradient,  $RRPG$ .

An experimental study reported measured water Amott wettability index ( $I_w$ ) for their carbonate-water-oil systems and demonstrated that  $\zeta_{m-p}$  became progressively more different from  $\zeta_{r-w}$  as  $I_w$  became smaller, reflecting more oil-wet conditions (Jackson et al., 2016). Consistent with their results, we assumed that the change in the

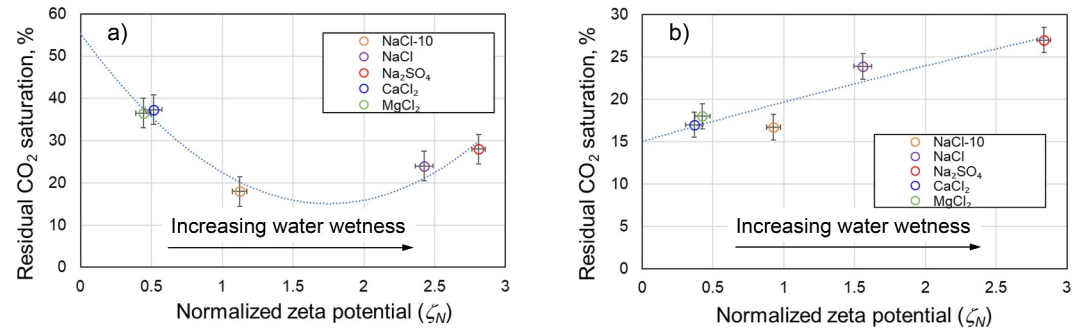


**Figure 7.** Residual CO<sub>2</sub> saturation versus normalized zeta potential defined by Equation 4 after (a) single rate imbibition (step 5), and (b) multi-rate paired stabilized experiments (step 6).

zeta potential in our experiments, ( $|\Delta\zeta_{wett}| = |\zeta_{r-w} - \zeta_{m-p}|$ ), also increased with a transition toward more scCO<sub>2</sub>-wet (less water-wet) state. Another study reported small  $|\Delta\zeta_{wett}|$  for (near) intermediate wettability (Collini et al., 2020). Therefore, small values of  $|\Delta\zeta_{wett}|$  in our experiments were expected to correspond to either strongly or weakly water-wet conditions.

On the other hand, small values of  $|\Delta\zeta_{wett}|$  could be comparable with the measurement error, hence suggesting  $|\Delta\zeta_{wett}|$  to be effectively zero. Therefore, we considered  $|\Delta\zeta_{wett}|$  in comparison with the experimental uncertainty, and scaled  $|\Delta\zeta_{wett}|$  by the reported errors in the respective multi-phase experiments,  $|\delta\zeta_{1-S_{gr}}|$ , to define  $\zeta_{RS}$ .

$$\zeta_{RS} = \left( \frac{|\Delta\zeta_{wett}|}{|\delta\zeta_{1-S_{gr}}|} \right)^{-1} \quad (2)$$

In Equation 2, the experimental uncertainties caused by the noise level, repeatability and instrument accuracy were evaluated as:  $\zeta_{1-S_{gr}} = \frac{\delta^+ + \delta^-}{2}$  with  $\delta^+$  and  $\delta^-$  corresponding to positive and negative experimental errors in  $\zeta_{m-p}$ .

Distinguishing between five different wetting states: strongly water-wet (SWW), weakly water-wet (WWW), intermediate-wet (IW), weakly CO<sub>2</sub>-wet (WCW), and strongly CO<sub>2</sub>-wet (SCW), this scaling resulted in the largest  $\zeta_{RS}$  to correspond to SWW conditions and the smallest  $\zeta_{RS}$ —the SCW state.

To allow a better distinction between WWW, IW and WCW conditions, we employed an additional independent wettability identifier, *RRPG*. Wettability is known to affect the shape of the relative permeability curves. Specifically, an increase in scCO<sub>2</sub> wetness results in an increase in the end-point relative permeability to water ( $k_{rw}^e$  at  $S_w = 1 - S_{gr}$ ) and a decrease in  $S_{gr}$  (Owens & Archer, 1971). Therefore, SWW systems should usually correspond to the lowest  $k_{rw}^e$  and highest  $S_{gr}$ , while IW, WCW and SCW systems should exhibit high  $k_{rw}^e$  and low  $S_{gr}$  (Heaviside et al., 1987). Thus, as a first order approach, the gradient of the relative permeability to water is expected to increase with increasing scCO<sub>2</sub> wetness, and the corresponding *RRPG*, defined by Equation 3, is expected to decrease.

$$RRPG = \left[ \frac{k_{rw}^e}{(1 - S_{gr} - S_{wirr})} \right]^{-1} \quad (3)$$

The assumption was experimentally confirmed by the experimental data presented in Figure 3b, where the lowest *RRPG* was observed in CaCl<sub>2</sub> and MgCl<sub>2</sub> systems. Furthermore, it is generally agreed that maximum gas recovery (minimum  $S_{gr}$ ) corresponds to IW state, when there is no specific affinity of the solid toward water or gas (Muggeridge et al., 2014). Therefore, we expect the lowest  $S_{gr}$  (largest  $S_w = 1 - S_{gr}$ ) to be reached for such wetting conditions. For the five distinct wetting conditions defined above, and considering the experimental uncertainty in  $S_w$  of c.10%. Thus, combining *RRPG* and  $\zeta_{RS}$ , each of which reflects wettability, allowed making a better distinction between different wetting states through the normalized zeta potential,  $\zeta_N$ :

$$\zeta_N = \zeta_{RS} \times RRP G = \left( \frac{|\Delta \zeta_{wett}|}{|\delta \zeta_{1-S_{gr}}|} \times \frac{k_{rw}^e}{(1 - S_{gr} - S_{wirr})} \right)^{-1} \quad (4)$$

The product of  $\zeta_{RS}$  and  $RRPG$ , both of which are the smallest for SCW and largest for SWW states, enhanced the distinction between wetting conditions as demonstrated in Figure 7. Since both,  $RRPG$  and  $\zeta_{RS}$  vary between zero and one with the smallest values of both properties corresponding to the least water-wet conditions, the expected correlation between the wetting state and  $\zeta_N$  is:

- $\zeta_N \gg 1$  in SWW systems.
- $\zeta_N \cong 1$  in WWW, IW, WCW systems.
- $\zeta_N \ll 1$  in SCW systems.

As described above, the implementation of high-rate bumps followed by multi-rate paired-stabilized experiments to evaluate  $\zeta_{m-p}$  resulted in additional production of  $\text{scCO}_2$  in tested  $\text{CaCl}_2$  and  $\text{MgCl}_2$  systems (and to a lesser extent with  $\text{NaCl-10}$ ) with the corresponding increase in  $k_{rw}^e$  (evaluated from the Darcy's law in our experiments), which indicated an existing capillary end effects, reduced or eliminated by high-rate injections. In Figure 7a,  $k_{rw}^e$  used in Equation 4 for  $\text{CaCl}_2$  and  $\text{MgCl}_2$  were computed using the data obtained from the single-rate injection corresponding  $\Delta S_w \cong 0.3$  in Figure 4b. For  $\text{CaCl}_2$ ,  $\text{MgCl}_2$  and  $\text{NaCl-10}$  data points in Figure 7b we used values of  $k_{rw}^e$  obtained at the end of all high-rate experiments (step 6) which correspond to  $\Delta S_w \cong 0.5$  in Figure 4b, while  $\Delta S_w$  was measured only after the first high-rate bump as detailed in the experimental protocol. Therefore, although the reported values in Figure 7b do not correspond to the same experimental conditions, the results are still valid as  $k_{rw}^e$ , which was continuously monitored throughout the entire step 6 of the experiment, did not vary beyond the experimental error. The overall  $RRPG$  in  $\text{CaCl}_2$ ,  $\text{MgCl}_2$  and  $\text{NaCl-10}$  experiments slightly decreased after high-rate experiments, thus supporting our hypothesis of existing capillary end effects and therefore, wettability alteration toward less water-wet, caused by presence of  $\text{scCO}_2$  in contact with solutions containing divalent cations and/or higher pore pressure. These results are consistent with the majority of reported contact angles measurement at CGS conditions (e.g., AL-Yaseri et al., 2016).

The effect of reduced or eliminated capillary end effect by high-rate bumps in  $\text{NaCl-10}$ ,  $\text{CaCl}_2$  and  $\text{MgCl}_2$  experiments is reflected by the overall change the correlation between  $\zeta_N$  and  $S_{gr}$  as demonstrated in Figure 7b. The lower values of  $S_{gr}$ , especially significant in  $\text{CaCl}_2$  and  $\text{MgCl}_2$  experiments, combined with the smallest  $\zeta_N < 1$  suggests that these systems were the least water-wet, while  $\zeta_N > 1$  for  $\text{Na}_2\text{SO}_4$  experiments corresponding to WWW or SWW conditions. Furthermore, the lowest  $S_{gr}$  in  $\text{Na}_2\text{SO}_4$  system observed in both after single-rate (Figure 7a) and high-rate (Figure 7b) experiments suggests small capillary end effects. At the same time the capillary end effects were significant in  $\text{CaCl}_2$  and  $\text{MgCl}_2$  systems, thus resulting in a substantial decrease in  $S_{gr}$  when transitioning from single-rate displacement (Figure 7a) to the high-rate bump (Figure 7b). Nonetheless, the final values of  $S_{gr}$  in  $\text{CaCl}_2$ ,  $\text{MgCl}_2$  and  $\text{NaCl-10}$  were equal and the lowest, suggesting similar wetting conditions. Also, a small change in  $\zeta_{m-p}$  (although within the experimental uncertainty) between the single-rate injection (Figure 7a) and high-rate bump (Figure 7b) carried out with  $\text{NaCl}$  solution resulted in a decrease in  $\zeta_N$  from  $\sim 2.5$  to  $\sim 1.5$ . All in all, considering the values of  $\zeta_N$  in the range between  $\sim 0.5$  and  $\sim 1.5$  for  $\text{NaCl}$ ,  $\text{NaCl-10}$ ,  $\text{CaCl}_2$  and  $\text{MgCl}_2$  systems. Incorporating the above observations, we concluded:

1.  $\text{CaCl}_2$ ,  $\text{MgCl}_2$ , and  $\text{NaCl-10}$ , all corresponded to IW conditions with the smallest  $\zeta_N = 0.37$ ,  $\zeta_N = 0.43$ , and  $\zeta_N = 0.93$ , respectively. This conclusion is consistent with results reported by Bikkina (2011) who measured contact angles of approximately  $82^\circ$ – $95^\circ$  on quartz substrates in contact with water and  $\text{scCO}_2$  at temperature of  $40^\circ\text{C}$  ( $104^\circ\text{F}$ ) and pressures between 7 MPa (1,000 psi) and 10 MPa (1,500 psi). The results also agree with the findings of Iglauer et al. (2012) who reported contact angles of  $80^\circ$  in quartz- $\text{scCO}_2$ -water systems at 300K and pressures between 7.5 and 10 MPa. The conclusion is also consistent with contact angles of  $\sim 80^\circ$  obtained on glass in contact with  $\text{scCO}_2$  and de-ionized water at conditions of temperature and pressure similar to those in our experiments (Sutjiadi-Sia et al., 2008). Our experimental results were used in a recent analytical study which reported that the maximum contact angles of approximately  $65^\circ$  could be achieved with DLVO model for  $\text{CaCl}_2$  and  $\text{MgCl}_2$  solutions (Vinogradov, 2024), thus confirming our conclusions. Directly measured contact angles of quartz in contact with  $\text{NaCl}$ ,  $\text{CaCl}_2$ , and  $\text{MgCl}_2$  were reported to have larger values for  $\text{CaCl}_2$  (c.  $43^\circ$ ) and  $\text{MgCl}_2$  (c.  $45^\circ$ ) compared with a smaller value for  $\text{NaCl}$  (c.  $36^\circ$ ) (AL-Yaseri et al., 2016). Although

these results are consistent with our interpretation of the shift toward more scCO<sub>2</sub>-wet conditions with CaCl<sub>2</sub> and MgCl<sub>2</sub>, the contact angles reported by Al-Yaseri et al. (2016) suggest that their systems remained water-wet, and significantly larger contact angles were reported in other studies. Another study of quartz in contact with live NaCl solutions and immiscible scCO<sub>2</sub> indicated, that although the system remained water-wet across the range of tested pressures, the contact angles shifted from approximately 50° at 7.5 MPa to approximately 70° at 10 MPa (Iglauer et al., 2012). This observation is consistent with our hypothesis of the shift from WWW state obtained with NaCl at 7.5 MPa to IW condition with NaCl at 10 MPa (note, that the contact angle of 70° is close to the value of 80°–100°, typically assigned for IW rocks).

2. Na<sub>2</sub>SO<sub>4</sub> corresponded to SWW conditions with the largest  $\zeta_N = 2.48$ , also confirmed by a significantly higher  $S_{gr} = 26\%$ . We could not find any measurements of contact angles on silica surfaces in contact with scCO<sub>2</sub> and Na<sub>2</sub>SO<sub>4</sub> to confirm this hypothesis. However, in line with the DLVO theory applied to the stability of the water wetting film (Tokunaga, 2012), stronger repulsive electrostatic forces between scCO<sub>2</sub>-C<sub>water</sub> and C<sub>water</sub>-quartz interfaces should result in a more water-wet conditions. Hence, the most negative  $\zeta_{r-w}$  obtained with Na<sub>2</sub>SO<sub>4</sub> in our work is consistent with our conclusion.
3. NaCl corresponded to WWW conditions with  $\zeta_N = 1.56$  and  $S_{gr} = 24\%$ , both of which indicate a lesser affinity toward water compared to Na<sub>2</sub>SO<sub>4</sub> results and higher water wetness compared with NaCl-10, CaCl<sub>2</sub>, and MgCl<sub>2</sub>. This conclusion is supported by numerous experimental studies that reported increasing contact angle with increasing pore pressure (e.g., Iglauer et al., 2012). Moreover, there have been many studies that also reported larger contact angles in quartz-scCO<sub>2</sub> with Ca/MgCl<sub>2</sub> solutions in comparison with NaCl solutions.

To validate our results and hypotheses, future work is planned to expand experiments toward higher salinity, mixed salts, direct measurements of  $\zeta_{c-w}$  and accurate evaluation of residual CO<sub>2</sub> saturation using X-ray computer tomography.

## 5. Conclusions

1. First ever  $\zeta_{m-p}$  measurements in scCO<sub>2</sub>-C<sub>water</sub>-silica systems were carried out following novel experimental protocols, the obtained results provided essential insights into controls on wettability and improved our understanding of previously unexplained differences in wetting states measured with different salts and experimental conditions.
2. For the first time  $\zeta_{c-w}$  was interpreted from measured experimental parameters and found to be negative and of magnitude greater than 14 mV.
3. We reported  $k_{rw}^e$  and respective residual scCO<sub>2</sub> saturation values at two stages of the experiment: at the end of single-rate imbibition mimicking CO<sub>2</sub> injection under capillary dominated regime, and after implementation of high-rate bumps and multi-rate paired-stabilized experiments which reduced the capillary end effects and provided additional data on intermediate relative permeability values in NaCl-10, CaCl<sub>2</sub> and MgCl<sub>2</sub> systems.
4. Wettability interpreted from  $\zeta_{r-w}$ ,  $\zeta_{m-p}$ , and  $k_{rw}^e$  measurements suggested IW conditions for NaCl-10, CaCl<sub>2</sub>, and MgCl<sub>2</sub>, SWW conditions for Na<sub>2</sub>SO<sub>4</sub> and WWW conditions for NaCl.
5. The introduced  $\zeta_N$  which comprises the scaled  $|\Delta\zeta_{well}|$  and relative permeability curve gradient, which are independent wettability indicators, has been proven as sufficient to distinguish between different wetting states without employing direct wettability measurements;  $\zeta_N$  also correlates well with  $S_{gr}$ , thus providing a powerful experimental tool to evaluate residual CO<sub>2</sub> trapping in sandstone reservoirs prior to injection for CGS.
6. There has been only one study that reported contact angles >90° in quartz-scCO<sub>2</sub>-C<sub>water</sub> systems (Bikina, 2011), thus reflecting WCW conditions. Nonetheless, we believe that presence of divalent cations in CaCl<sub>2</sub> and MgCl<sub>2</sub> experiments combined with the low ionic strength of 0.05 M might have created WCW conditions, consistent with  $\zeta_N < 1$  and low  $S_{gr}$ .

## Conflict of Interest

The authors declare no conflicts of interest relevant to this study.

## Data Availability Statement

The underlying data are available at Vinogradov et al. (2024).

**Acknowledgments**

Miftah Hidayat was supported by the Aberdeen-Curtin PhD studentship. David Vega-Maza is funded by the Spanish Ministry of Science, Innovation and Universities (“Beatriz Galindo Senior” fellowship BEAGAL18/00259).

**References**

Ali, M., Jha, N. K., Pal, N., Keshavarz, A., Hoteit, H., & Sarmadivaleh, M. (2022). Recent advances in carbon dioxide geological storage, experimental procedures, influencing parameters, and future outlook. *Earth-Science Reviews*, 225, 103895. <https://doi.org/10.1016/j.earscirev.2021.103895>

Alnili, F., Al-Yaseri, A., Roshan, H., Rahman, T., Verall, M., Lebedev, M., et al. (2018). Carbon dioxide/brine wettability of porous sandstone versus solid quartz: An experimental and theoretical investigation. *Journal of Colloid and Interface Science*, 524, 188–194. <https://doi.org/10.1016/j.jcis.2018.04.029>

Al-Yaseri, A., Lebedev, M., Barifcani, A., & Iglauer, S. (2016). Receding and advancing CO<sub>2</sub>-brine-quartz contact angles as a function of pressure, temperature, surface roughness, salt type and salinity. *The Journal of Chemical Thermodynamics*, 93, 416–423. <https://doi.org/10.1016/j.jct.2015.07.031>

Benson, S. M., & Cole, D. R. (2008). CO<sub>2</sub> sequestration in deep sedimentary formations. *Elements*, 4(5), 325–331. <https://doi.org/10.2113/gselements.4.5.325>

Bikkina, P. K. (2011). Contact angle measurements of CO<sub>2</sub>-water-quartz/calcite systems in the perspective of carbon sequestration. *International Journal of Greenhouse Gas Control*, 5(5), 1259–1271. <https://doi.org/10.1016/j.ijggc.2011.07.001>

Blunt, M. J., Bijeljic, B., Dong, H., Gharbi, O., Iglauer, S., Mostaghimi, P., et al. (2013). Pore-scale imaging and modelling. *Advances in Water Resources*, 51, 197–216. <https://doi.org/10.1016/j.advwatres.2012.03.003>

Chen, C., Wan, J., Li, W., & Song, Y. (2015). Water contact angles on quartz surfaces under supercritical CO<sub>2</sub> sequestration conditions: Experimental and molecular dynamics simulation studies. *International Journal of Greenhouse Gas Control*, 42, 655–665. <https://doi.org/10.1016/j.ijggc.2015.09.019>

Chiquet, P., Broseta, D., & Thibeau, S. (2007). Wettability alteration of caprock minerals by carbon dioxide. *Geofluids*, 7(2), 112–122. <https://doi.org/10.1111/j.1468-8123.2007.00168.x>

Collini, H., & Jackson, M. D. (2022). Relationship between zeta potential and wettability in porous media: Insights from a simple bundle of capillary tubes model. *Journal of Colloid and Interface Science*, 608, 605–621. <https://doi.org/10.1016/j.jcis.2021.09.100>

Collini, H., Li, S., Jackson, M. D., Agenet, N., Rashid, B., & Couves, J. (2020). Zeta potential in intact carbonates at reservoir conditions and its impact on oil recovery during controlled salinity waterflooding. *Fuel*, 266, 116927. <https://doi.org/10.1016/j.fuel.2019.116927>

Heaviside, J., Brown, C. E., & Gamble, I. J. (1987). Relative permeability for intermediate wettability reservoirs. In *In SPE annual technical conference and exhibition*. OnePetro.

Hidayat, M., Sarmadivaleh, M., Derksen, J., Vega-Maza, D., Iglauer, S., & Vinogradov, J. (2022a). Zeta potential of CO<sub>2</sub>-rich aqueous solutions in contact with intact sandstone sample at temperatures of 23°C and 40°C and pressures up to 10.0 MPa. *Journal of Colloid and Interface Science*, 607, 1226–1238. <https://doi.org/10.1016/j.jcis.2021.09.076>

Hidayat, M., Sarmadivaleh, M., Derksen, J., Vega-Maza, D., Iglauer, S., & Vinogradov, J. (2022b). Zeta potential of a natural clayey sandstone saturated with carbonated NaCl solutions at supercritical CO<sub>2</sub> conditions. *Geophysical Research Letters*, 49(15), e2022GL099277. <https://doi.org/10.1029/2022gl099277>

Hirasaki, G. J. (1991). Wettability: Fundamentals and surface forces. *SPE Formation Evaluation*, 6(02), 217–226. <https://doi.org/10.2118/17367-pa>

Iglauer, S., Mathew, M., & Bresme, F. (2012). Molecular dynamics computations of brine-CO<sub>2</sub> interfacial tensions and brine-CO<sub>2</sub>-quartz contact angles and their effects on structural and residual trapping mechanisms in carbon geo-sequestration. *Journal of Colloid and Interface Science*, 386(1), 405–414. <https://doi.org/10.1016/j.jcis.2012.06.052>

Iglauer, S., Pentland, C. H., & Busch, A. (2015). CO<sub>2</sub> wettability of seal and reservoir rocks and the implications for carbon geo-sequestration. *Water Resources Research*, 51(1), 729–774. <https://doi.org/10.1002/2014wr015553>

Jackson, M. D., Al-Mahrouqi, D., & Vinogradov, J. (2016). Zeta potential in oil-water-carbonate systems and its impact on oil recovery during controlled salinity water-flooding. *Scientific Reports*, 6, 1–13. <https://doi.org/10.1038/srep37363>

Jung, J. W., & Wan, J. (2012). Supercritical CO<sub>2</sub> and ionic strength effects on wettability of silica surfaces: Equilibrium contact angle measurements. *Energy & Fuels*, 26(9), 6053–6059. <https://doi.org/10.1021/ef300913t>

Kim, M. S., & Kwak, D. H. (2017). Effect of zeta potential on collision-attachment coefficient and removal efficiency for dissolved carbon dioxide flotation. *Environmental Engineering Science*, 34(4), 272–280. <https://doi.org/10.1089/ees.2016.0325>

Krevor, S. C., Pini, R., Zuo, L., & Benson, S. M. (2012). Relative permeability and trapping of CO<sub>2</sub> and water in sandstone rocks at reservoir conditions. *Water Resources Research*, 48(2), W02532. <https://doi.org/10.1029/2011wr010859>

McBride-Wright, M., Maitland, G. C., & Trusler, J. P. M. (2015). Viscosity and density of aqueous solutions of carbon dioxide at temperatures from (274 to 449) K and at pressures up to 100 MPa. *Journal of Chemical & Engineering Data*, 60(1), 171–180. <https://doi.org/10.1021/je5009125>

Moore, J. R., Glaser, S. D., Morrison, H. F., & Hoversten, G. M. (2004). The streaming potential of liquid carbon dioxide in Berea sandstone. *Geophysical Research Letters*, 31(17), L17610. <https://doi.org/10.1029/2004gl020774>

Muggeridge, A., Cockin, A., Webb, K., Frampton, H., Collins, I., Moulds, T., & Salino, P. (2014). Recovery rates, enhanced oil recovery and technological limits. *Philosophical Transactions of the Royal Society A*, 372(2006), 20120320. <https://doi.org/10.1098/rsta.2012.0320>

Najafi, A. S., Drelich, J., Yeung, A., Xu, Z., & Masliyah, J. (2007). A novel method of measuring electrophoretic mobility of gas bubbles. *Journal of Colloid and Interface Science*, 308(2), 344–350. <https://doi.org/10.1016/j.jcis.2007.01.014>

Owens, W. W., & Archer, D. (1971). The effect of rock wettability on oil-water relative permeability relationships. *Journal of Petroleum Technology*, 23(07), 873–878. <https://doi.org/10.2118/3034-pa>

Sarmadivaleh, M., Al-Yaseri, A. Z., & Iglauer, S. (2015). Influence of temperature and pressure on quartz–water–CO<sub>2</sub> contact angle and CO<sub>2</sub>-water interfacial tension. *Journal of Colloid and Interface Science*, 441, 59–64. <https://doi.org/10.1016/j.jcis.2014.11.010>

Silvestri, A., Ataman, E., Budi, A., Stipp, S. L. S., Gale, J. D., & Raiteri, P. (2019). Wetting properties of the CO<sub>2</sub>-water-calcite system via molecular simulations: Shape and size effects. *Langmuir*, 35(50), 16669–16678. <https://doi.org/10.1021/acs.langmuir.9b02881>

Singh, K., Bijeljic, B., & Blunt, M. J. (2016). Imaging of oil layers, curvature and contact angle in a mixed-wet and a water-wet carbonate rock. *Water Resources Research*, 52(3), 1716–1728. <https://doi.org/10.1002/2015wr018072>

Song, J., Zeng, Y., Wang, L., Duan, X., Puerto, M., Chapman, W. G., et al. (2017). Surface complexation modeling of calcite zeta potential measurements in brines with mixed potential determining ions (Ca<sup>2+</sup>, CO<sub>3</sub><sup>2-</sup>, Mg<sup>2+</sup>, SO<sub>4</sub><sup>2-</sup>) for characterizing carbonate wettability. *Journal of Colloid and Interface Science*, 506, 169–179. <https://doi.org/10.1016/j.jcis.2017.06.096>

Stevan, M. S., Böhm, C., Notarki, K. T., & Trusler, J. M. (2019). Wettability of calcite under carbon storage conditions. *International Journal of Greenhouse Gas Control*, 84, 180–189. <https://doi.org/10.1016/j.ijggc.2019.03.024>

- Sutjiadi-Sia, Y., Jaeger, P., & Eggers, R. (2008). Interfacial phenomena of aqueous systems in dense carbon dioxide. *The Journal of Supercritical Fluids*, 46(3), 272–279. <https://doi.org/10.1016/j.supflu.2008.06.001>
- Tokunaga, T. K. (2012). DLVO-based estimates of adsorbed water film thicknesses in geologic CO<sub>2</sub> reservoirs. *Langmuir*, 28(21), 8001–8009. <https://doi.org/10.1021/la2044587>
- Tudek, J., Crandall, D., Fuchs, S., Werth, C. J., Valocchi, A. J., Chen, Y., & Goodman, A. (2017). In situ contact angle measurements of liquid CO<sub>2</sub>, brine, and Mount Simon sandstone core using micro X-ray CT imaging, sessile drop, and Lattice Boltzmann modeling. *Journal of Petroleum Science and Engineering*, 155, 3–10. <https://doi.org/10.1016/j.petrol.2017.01.047>
- Vinogradov, J. (2024). Wettability of quartz sandstone in contact with supercritical CO<sub>2</sub> and aqueous solutions—novel insights from updated DLVO model. *Journal of Clean Energy and Energy Storage*, 01. <https://doi.org/10.1142/S2811034X24500047>
- Vinogradov, J., Hidayat, M., Sarmadivaleh, M., Derksen, J., Vega-Maza, D., Iglauer, S., et al. (2022). Predictive surface complexation model of the calcite-aqueous solution interface: The impact of high concentration and complex composition of brines. *Journal of Colloid and Interface Science*, 609, 852–867. <https://doi.org/10.1016/j.jcis.2021.11.084>
- Vinogradov, J., Hidayat, M., Sarmadivaleh, M., Vega-Maza, D., Iglauer, S., Zhang, L., et al. (2024). Zeta potential of supercritical CO<sub>2</sub>-water-sandstone systems and its correlation with wettability and residual subsurface trapping of CO<sub>2</sub> [Dataset]. *OSF*. <https://doi.org/10.17605/OSF.IO/HW4TM>
- Vinogradov, J., Hill, R., & Jougnot, D. (2021). Influence of pore size distribution on the electrokinetic coupling coefficient in two-phase flow conditions. *Water*, 13(17), 2316. <https://doi.org/10.3390/w13172316>
- Vinogradov, J., Jaafar, M. Z., & Jackson, M. D. (2010). Measurement of streaming potential coupling coefficient in sandstones saturated with natural and artificial brines at high salinity. *Journal of Geophysical Research*, 115(B12), B12204. <https://doi.org/10.1029/2010jb007593>
- Vinogradov, J., & Jackson, M. D. (2011). Multiphase streaming potential in sandstones saturated with gas/brine and oil/brine during drainage and imbibition. *Geophysical Research Letters*, 38(1), L01301. <https://doi.org/10.1029/2010gl045726>
- Yong, W., Derksen, J., & Zhou, Y. (2021). The influence of CO<sub>2</sub> and CH<sub>4</sub> mixture on water wettability in organic rich shale nanopore. *Journal of Natural Gas Science and Engineering*, 87, 103746. <https://doi.org/10.1016/j.jngse.2020.103746>
- Zhou, Y., Han, Z., He, C., Feng, Q., Wang, K., Wang, Y., et al. (2021). Long-term stability of different kinds of gas nanobubbles in deionized and salt water. *Materials*, 14(7), 1808. <https://doi.org/10.3390/ma14071808>